Journal of Polymers and the Environment (2024) 32:3313–3325
https://doi.org/10.1007/s10924-023-03155-8

ORIGINAL PAPER

Improvement of Cross-linked Alginate Hydrogel Microparticles Loaded with Galangin-β-Cyclodextrin Complex by Response Surface Methodology

Saliha Şahin[1] · Önder Aybastıer[1] · Eftal Alp Dorken[1] · İlkyaz Patır[1]

Accepted: 6 December 2023 / Published online: 21 January 2024
© The Author(s) 2024

Abstract
Galangin is a phenolic compound with antioxidant and anti-tyrosinase activity, which makes it highly useful in cosmetics and medicine. However, the poor solubility of galangin in water limits its usefulness in these areas. This study it is aimed to increase the solubility of galangin in water by encapsulation method. Therefore, in this study, ethanolic and methanolic extracts were obtained from *Alpinia officinarum* Hance, and the phenolic compound profile and content of the extracts were determined by HPLC-DAD. Galangin was purified and fractionated from *Alpinia officinarum* Hance extracts by column chromatography. Galangin was encapsulated with β-cyclodextrin, and galangin-β-cyclodextrin loaded alginate hydrogel microparticles were developed. The central composite design-response surface methodology was used to develop galangin-β-cyclodextrin loaded alginate hydrogel microparticles under optimum conditions with maximum galangin release. The encapsulation efficiency and release of galangin in galangin-β-cyclodextrin loaded alginate hydrogel microparticles developed under optimum conditions were characterized by HPLC-DAD, surface morphology by SEM, and structural properties by FTIR.

Keywords Hydrogel · Optimization · Microencapsulation · *Alpinia officinarum* · Galangin

Introduction

Alpinia officinarum Hance (smaller galanga; AO) is a member of the *Zingiberaceae* family, which has rhizomes with dark brown-reddish color and aromatic odor, and its origin in Asian countries [1–3]. Its roots have been used for centuries as a fragrance and spice in food and as a drug for various diseases such as diabetes, ulcers, and bronchitis in traditional medicine [4, 5]. AO has a wide variety of bioactive components, for instance, proteins, amino acids, alkaloids, sterols, saponins, phenylpropanoids, diarylheptanoids, and phenolic compounds [6]. Besides this, all its rich bioactive content, it has valuable flavonoid content, e.g., galangin, 3-O-methyl galangin, kaempferide, isorhamnetin, quercetin, and kaempferol [7, 8].

Galangin (GAL) is the main component of *Alpinia officinarum* Hance. GAL belongs to the class of flavonols from flavonoids [9]. Many studies have revealed that GAL has antioxidant, anti-inflammatory, antimicrobial, antiarthritis, anticancer, neuroprotective, hepatoprotective, anti-atopic dermatitis, and anti-wrinkle properties [10, 11]. However, the fact that GAL is a weakly acidic compound and not easily soluble in water is the reason why it is the most lipophilic compound among flavonoids such as quercetin, kaempferol, morin, and myricetin [12]. Due to its poor solubility in water, GAL has low bioaccessibility and bioavailability, and therefore the medicinal use of GAL is limited [13].

Active substances such as GAL, which have medicinally beneficial properties but whose use is very limited due to poor solubility, low bioavailability, etc., can be loaded into various carrier systems using encapsulation. In order to utilize the biological activities of galangin more effectively,

✉ Saliha Şahin
salihabilgi@uludag.edu.tr

Önder Aybastıer
aybastier@uludag.edu.tr

Eftal Alp Dorken
eftalalpdorken@gmail.com

İlkyaz Patır
ilkyazpatir@gmail.com

[1] Department of Chemistry, Faculty of Science and Arts, Bursa Uludag University, Bursa, Türkiye

carrier systems have been developed using various encapsulation techniques in the literature. These include liposomes [14–18], niosomes [13], micelles [19, 20], emulsions [21], nanoparticles [22–25], cyclodextrin complexes [26, 27] and hydrogels [28]. The authors reported that with the carrier systems used, the limitation of low bioavailability as a result of the hydrophobic property of galangin was overcome, and the targeted biological activity was increased [29].

Hydrogels are hydrophilic, three-dimensional structures consisting of cross-linked polymer networks. The hydrophilic nature of hydrogels enables them to hold a high proportion of water in their structure [30]. Hydrogels have an advantageous properties such as high water absorption capacity, elastic structure, biocompatibility, low toxicity, easy functionalization, targeted delivery, and controlled drug release [31]. Hydrogels are mainly formed from polymers/polymer blends and cross-linkers. Synthetic and natural polymers can be used in the production of hydrogels. The most commonly used natural polymers are alginate, collagen, chitosan, hyaluronic acid, gelatin, and the most commonly used synthetic polymers are polyethylene glycol derivatives, polyvinylalcohol, polyurethane, and polycaprolactone [32].

Sodium alginate is the sodium salt form of alginic acid from marine algae and has a hydrophilic structure. Alginic acid is a linear block copolymer polysaccharide consisting of β-D-mannuronic acid and α-L-glucuronic acid residues joined by 1,4-glycosidic linkages and has high gelling ability. Alginate interacts strongly with cations and has strong cross-linking ability. It is most commonly used with calcium ions as a cross-linker, and ion exchange occurs between calcium and alginate during gel formation, calcium ions form the egg-box structure with carboxyl and hydroxyl groups in alginate. Hydrogels are produced by chemical cross-linking techniques with covalent bonds and physical cross-linking techniques with hydrogen bonding, electrostatic and hydrophobic interactions [33]. Therefore, it is very suitable for hydrogel formation. In addition, it is frequently used in hydrogel production because it is non-toxic, biocompatible, and provides high water absorption capacity due to the extensive hydrogel network it forms when cross-linked [34].

Hydrogels can be designed in macro, micro, and nano size with various strategies and techniques. The macro-size range of mm to cm and micro-size range of 1-1000 µm are called microgels or hydrogel microparticles. Due to their small size, hydrogel microparticles have a large surface area and polymeric network to interact with drugs and load drugs into their centers [35, 36]. Under these properties, hydrogel microparticles (HMPs) are often preferred in developing controlled and sustained release delivery systems of nanoparticles, living cells, and drugs [37]. In addition, HMPs are frequently used as carrier systems for phenolic compounds, nutritional and flavor components, which have therapeutic effects but have low bioavailability, solubility, and stability in environmental conditions [38]. HMPs play an active role in developing drugs and injectable gels for medical applications and creams and gels for cosmetic applications [39, 40].

GAL is a phenolic compound suitable for cosmetics due to its antioxidant, antimicrobial, anti-wrinkle, anti-tyrosinase, and antimelanogenic activities. However, due to the low solubility and release rate of GAL, it cannot be used effectively without carrier systems. Therefore, in this study, hydrogel microparticles (GAL-β-CD-ALG HMPs) were developed with GAL-β-CD encapsulate. Unlike the other studies in the literature given above, galangin complex was formed with β-CD, whose outer surface is hydrophilic but the cavity on the inner surface is hydrophobic, and this complex was loaded into the hydrogel network formed with alginate. Due to the poor ability of hydrogels formed with alginate to encapsulate small-size molecules, galangin-β-CD complex was constructed. While the hydrophilic region of β-CD interacts with the hydrogel network, the hydrophobic cavity interacts with galangin. Considering this theory, high encapsulation efficiency and increasing the solubility and release of GAL was targeted. The encapsulation efficiency, surface morphology, size, and structural properties of obtained GAL-β-CD-ALG HMPs were characterized.

Materials and Methods

Materials

β-cyclodextrin, acetonitrile, alginic acid sodium salt, *p*-coumaric acid, quercetin, and kaempferol were purchased from Sigma-Aldrich (St. Louis, MO., USA). Ethanol, methanol, tri-sodium citrate dihydrate, calcium chloride dihydrate, and formic acid were purchased from Merck (Darmstadt, Germany). Citric acid monohydrate was purchased from Kimetsan. Galangin was purchased from Extrasynthese. *Alpinia officinarum* Hance root powder was purchased from a local market in Bursa, Türkiye.

Methods

Extraction of *Alpinia officinarum* Hance

To extract phenolic compounds from AO, 100 mL of solvent (80% EtOH or 80% MeOH) was added to 20 g of AO root powder. It was extracted at 10°C for 4 h and then filtered with filter paper (Whatman No.1) and stored at 4°C until use [41].

Chromatographic Analysis

The determination of phenolic compound profile and quantitation was studied by HPLC-DAD (Agilent 1200 Series,

USA) using the Karkar et al., method. The chromatographic separations of phenolic compounds were performed using an XBridge® C18 (4.6×250 mm, 3.5 µm) column (Waters, USA). The gradient mobile phase contained 1% formic acid (solvent A) and acetonitrile (solvent B) in water, the flow rate was 0.5 mL/min, the column temperature was 25 °C, and the injection volume of samples was 10 µL. The quantitation of phenolic compounds was calculated by the standard calibration graph of phenolic compounds [42].

Fractionation of *Alpinia officinarum* Hance by Column Chromatography

The purification and fractionation of 80% ethanolic and 80% methanolic extract of AO were studied by column chromatography. Briefly, the glass column was filled with Sephadex LH-20 and connected to a peristaltic pump (Watson Marlow, USA). Then, 10 mL of extract (80% ethanolic and 80% methanolic extract) was passed through the column, followed by 100 mL of solvent (ethanol or methanol), and 3 mL of fractions were collected. After measuring the UV absorption of the obtained ethanolic and methanolic fractions at 320 and 360 nm by UV-Vis spectrophotometer (Varian, Cary 50 Conc) [43], the amount of phenolic compounds of fractions was analyzed by the HPLC-DAD method described in chromatographic analysis. The ethanolic and methanolic fractions of AO extracts obtained after purification by column chromatography were combined and used in further steps.

Hydrogel Microparticles-Based Encapsulation of GAL

For the encapsulation of GAL into HMPs, firstly GAL-β-cyclodextrin (GAL-β-CD) inclusion complex was generated. For the formation of the inclusion complex, GAL purified from ethanolic and methanolic extracts was used. To prepare the GAL-β-CD complex, 25 mg of GAL (purified from ethanol and methanol extract of AO extract) was added to 2 g of β-CD and stirred at 50°C with a magnetic stirrer until the solvent evaporated. The GAL-β-CD inclusion complex (GAL-β-CD) was obtained. For the preparation of HMPs, the GAL-β-CD (0.1–0.9%) and ALG (0.5–2.5%) solution were homogenized. The solution was added dropwise with an injector to 50 mL $CaCl_2$ (1.0–3.0%) solution stirred at 125 rpm for 10–50 min. The GAL-β-CD-ALG HMPs obtained at the end of the stirring process were filtered through filter paper, washed with 20 mL of distilled water, and dried at room temperature.

Experimental Design

In this study, four parameters (input factors), ALG quantity, $CaCl_2$ quantity, time, and GAL-β-CD quantity were selected to generate GAL-β-CD-ALG HMPs with maximum efficiency. In the experimental design, GAL release (output factor) was selected as the response. These parameters and their combinations were determined using Central Composite Design (CCD) to determine the optimum conditions required to achieve maximum GAL release [44, 45]. The ranges of the four parameters studied for the CCD are given in Table 1.

The total number of experiments (N) in a CCD can be calculated using the following Eq. (1):

$$N = 2^k + 2k + x_0 \quad (1)$$

where k represents the number of variables, and x_0 is the replicate number of the center point. In this study, CCD (five-level, four-factor) was applied, which required thirty experiments (six replicates) for the optimization of GAL-β-CD-ALG HMPs generation parameters (Table 2).

Multiple regression analysis was applied to the experimental data from the thirty experiments, and the following Eq. (2), including all interaction terms, was then used to calculate the predicted response:

$$y = b_0 + \sum_{i=1}^{4} b_i x_i + \sum_{i=1}^{4} b_{ii} x_i^2 + \sum_{i=1}^{3} \sum_{j=i+1}^{4} b_{ij} x_i x_j \quad (2)$$

where y is the response, b_0 is the constant, b_i, b_{ii}, b_{ij} are linear, quadratic, and interaction effects, respectively, and x_i and x_j are independent variables. The analysis of variance (ANOVA), regression analysis, and response surface plots were plotted using Design Expert 7.0.0 software (Stat-Ease Inc., USA) for statistical analysis results to determine the optimum conditions for HMPs generation.

Release Study of HMPs

GAL release (response of experimental design) of GAL-β-CD-ALG HMPs was determined by the chromatographic method described in chromatographic analysis. Briefly, 0.15 g of HMPs and 2 mL of citrate buffer (pH 5.5) were vortexed for 2 min and incubated at 37°C for 1 h. After

Table 1 Independent factors and their levels used for central composite design

Independent factor	Level				
	−2	−1	0	1	2
ALG quantity (w/v %)	0.5	1.0	1.5	2.0	2.5
$CaCl_2$ quantity (w/v %)	1.0	1.5	2.0	2.5	3.0
Time (min)	10	20	30	40	50
GAL-β-CD quantity (w/v %)	0.1	0.3	0.5	0.7	0.9

ALG Sodium alginate, *GAL-β-CD* β-cyclodextrin-GALencapsulate, *GAL* Galangin

Table 2 Central composite design of factors with coded values

Treatment	Factors			
	x_1	x_2	x_3	x_4
	ALG quantity (w/v %)	$CaCl_2$ quantity (w/v %)	Time (min)	GAL-β-CD quantity (w/v %)
1	1	1.5	20	0.3
2	2	1.5	20	0.3
3	1	2.5	20	0.3
4	2	2.5	20	0.3
5	1	1.5	40	0.3
6	2	1.5	40	0.3
7	1	2.5	40	0.3
8	2	2.5	40	0.3
9	1	1.5	20	0.7
10	2	1.5	20	0.7
11	1	2.5	20	0.7
12	2	2.5	20	0.7
13	1	1.5	40	0.7
14	2	1.5	40	0.7
15	1	2.5	40	0.7
16	2	2.5	40	0.7
17	0.5	2	30	0.5
18	2.5	2	30	0.5
19	1.5	1	30	0.5
20	1.5	3	30	0.5
21	1.5	2	10	0.5
22	1.5	2	50	0.5
23	1.5	2	30	0.1
24	1.5	2	30	0.9
25	1.5	2	30	0.5
26	1.5	2	30	0.5
27	1.5	2	30	0.5
28	1.5	2	30	0.5
29	1.5	2	30	0.5
30	1.5	2	30	0.5

incubation, the amounts of GAL remaining in the supernatant were determined by the HPLC-DAD method.

Characterization of HMPs

The GAL-β-CD-ALG HMPs samples were dried at room temperature for 24 h before the FTIR and SEM analysis.

FTIR Analysis

The structural characterization of GAL-β-CD-ALG HMPs was studied by FTIR spectrometer (Perkin Elmer, Spectrum 100, USA) in 400–4000 cm^{-1} frequency range.

SEM Analysis

The morphological characterization and size of GAL-β-CD-ALG HMPs were studied by SEM (Scanning Electron Microscopy, Carl Zeiss Evo 40, Germany) at 20.0 kV and 200 X-3.00 KX magnification. The dried hydrogels were placed on aluminum plates and covered with gold.

Encapsulation Efficiency

Encapsulation efficiency was determined by the release study of HMPs. Encapsulation efficiency was determined by this equation:

$$\text{Encapsulation efficiency}(\%) = \frac{W_{initial} - W_{free}}{W_{initial}} \times 100$$

$W_{initial}$: The initial amount of GAL, W_{free} : The released amount of GAL.

Result and Discussion

Determination and Quantitation of Phenolic Compound by HPLC-DAD

The phenolic compound profile of AO was determined by HPLC-DAD. According to HPLC analysis, 80% ethanolic and 80% methanolic extract contains GAL, *p*-coumaric acid, quercetin, and kaempferol. The most intense peak belongs to GAL, and GAL is the main component of AO. Similarly, Tao et al., reported that the methanolic extract of *Alpinia officinarum* Hance had two components, GAL and 3-*O*-methyl galangin, in the extract by HPLC analysis and that GAL was the main component [7]. The quantity of phenolic compounds in the extracts of AO was calculated using calibration graphs of phenolic compound standards. According to the results of the quantitative analysis of phenolic compounds, the AO ethanolic extract contains 11.4343 ± 0.0729 mg/g GAL, 6.1 ± 0.1 µg/g *p*-coumaric acid, 61.2 ± 1.5 µg/g quercetin and 219.9 ± 1.5 µg/g kaempferol. AO methanolic extract contains 10.4906 ± 0.1146 mg/g GAL, 3.1 ± 0.2 µg/g *p*-coumaric acid, 60.4 ± 0.2 µg/g quercetin and 196.8 ± 1.8 µg/g kaempferol. Pirzadeh et al., reported that the main components in the extract were GAL, kaempferol, and quercetin, and their amounts of 5.8 mg/g, 10.8 mg/g, and 4.25 mg/g as a result of HPLC analysis of the hydroalcoholic (40% ethanol) extract of *Alpinia officinarum* Hance [46]. Similarly, Li et al., showed that the main bioactive components of *Alpinia officinarum* Hance extract (95% ethanol) were quercetin, kaempferol, and galangin and explained that

galangin was the main component of the *Alpinia officinarum* Hance extract, similar to the result of our study [47].

Fractionation of *Alpinia officinarum* Hance

According to the data obtained from HPLC-DAD analysis, 0.4454 mg/g quercetin, 3.2345 mg/g kaempferol, 217.056 mg/g GAL, and 0.0102 mg/g *p*-coumaric acid was quantified in the ethanolic extract of AO after purification. The amount of quercetin 0.3842 mg/g, kaempferol 3.0146 mg/g, *p*-coumaric acid 0.0041 mg/g, and GAL in the extract increased by approximately 205 mg/g with the purification process. As a result of this increase, GAL constituted 98.33% of the phenolic compound content in the ethanolic extract. In the methanolic extract of AO, 0.3885 mg/g quercetin, 3.0028 mg/g kaempferol, 215.4150 mg/g GAL, and 0.0117 mg/g *p*-coumaric acid were determined after purification. The amount of quercetin 0.3281 mg/g, kaempferol 2.8060 mg/g, *p*-coumaric acid 0.0086 mg/g, and GAL in the extract increased by about 205 mg/g with the purification process. As a result of this increase, GAL constituted 98.44% of the phenolic compound content in the ethanolic extract. Fang et al., purified 99.30% galangin from the ethyl acetate fraction of the ethanolic extract of *Alpinia officinarum* Hance using high-speed counter-current chromatography (HSCCC). Although the method we used in our study is basically the same as HSCCC, it is much simpler than HSCCC and lacks automation, galangin was purified with 98.33% purity with a purity difference of about 1.00% [48].

Experimental Design

Fitting the Model

The generation parameters of GAL-β-CD-ALG HMPs were optimized by RSM-CCD. The optimum combination of ALG quantity (0.5–2.5%), $CaCl_2$ quantity (1.0–3.0%), time (10–50 min), and GAL-β-CD (0.1–0.9%) variables were investigated for the generation of HMPs with maximum GAL release. The coded values, experimental and predicted GAL release concentrations are given in Table 3. It was observed that the predicted and experimental values were compatible. Among the 30 experiments performed for optimization, experiment 23 had the lowest GAL release concentration; 0.84 mg/L, and experiment 17 had the highest GAL release concentration, 3.90 mg/L.

The Design Expert program (Version 7.0.0) was used to calculate each variable's effects and interactions with each other. ANOVA analysis and fitting the experimental data to the models showed that the GAL release concentration is defined by the quadratic polynomial model. In Table 4, the *p*-value for GAL release concentration was lower than 0.0001 ($p < 0.0001$). The *p*-value was used to describe the relationship between the response and variables in the quadratic polynomial model and was found to be significant. The F-value of the model was calculated as 12.56 and was considered significant at a 95% confidence level. The model's lack of fit *p*-value was calculated as 0.3641, indicating that the model was valid.

Table 3 Central composite design of factors with experimental and predicted values

Treatment	Concentration of released GAL (mg/L)	
	Experimental	Predicted
1	2.65	2.49
2	1.52	1.33
3	2.29	2.34
4	1.30	1.55
5	3.16	3.35
6	2.39	2.06
7	2.13	1.88
8	0.95	0.96
9	3.26	3.22
10	2.09	2.34
11	3.15	3.49
12	3.19	2.98
13	3.67	3.43
14	2.50	2.43
15	2.20	2.38
16	1.57	1.75
17	3.93	3.90
18	2.06	2.11
19	3.00	3.30
20	2.75	2.47
21	2.35	2.20
22	1.66	1.82
23	0.63	0.84
24	2.54	2.35
25	2.86	2.76
26	2.86	2.76
27	2.31	2.76
28	2.84	2.76
29	3.08	2.76
30	2.63	2.76

GAL Galangin

Response Surface Analysis

The effects of variables ALG quantity, $CaCl_2$ quantity, time, and GAL-β-CD for the generation of hydrogel microparticles were studied. The response surface analysis shows

Table 4 Analysis of variance (ANOVA) for the fitted quadratic polynomial model for optimization of encapsulation parameters

Source	Concentration of released GAL ($R^2 = 0.9214$)				
	DF	SS	MS	*F* value	*p* value
Model	14	15.58	1.11	12.56	< 0.0001
x_1	1	4.82	4.82	54.36	< 0.0001
x_2	1	1.03	1.03	11.61	0.0039
x_3	1	0.21	0.21	2.41	0.1414
x_4	1	3.44	3.44	38.79	< 0.0001
x_1x_2	1	0.14	0.14	1.55	0.2327
x_1x_3	1	0.015	0.015	0.17	0.6839
x_1x_4	1	0.081	0.081	0.92	0.3528
x_2x_3	1	1.74	1.74	19.69	0.0005
x_2x_4	1	0.17	0.17	1.92	0.1856
x_3x_4	1	0.42	0.42	4.78	0.0450
x_1^2	1	0.097	0.097	1.09	0.3123
x_2^2	1	0.024	0.024	0.27	0.6080
x_3^2	1	0.97	0.97	10.90	0.0048
x_4^2	1	2.34	2.34	26.43	0.0001
Lack of fit	10	0.98	0.098	1.43	0.3641
Pure error	5	0.34	0.069		

DF Degree of freedom; *SS* sum of squares; *MS* mean square

that the relationship between GAL release concentration and GAL-β-CD-ALG HMPs generation factors is quadratic and has a good regression coefficient of 0.9214 (Table 4). Table 5 gives the second-order polynomial equation for the GAL release concentration. According to the equation, x_1 (ALG quantity (w/v %)), x_2 ($CaCl_2$ quantity (w/v %)), x_4 (GAL-β-CD (w/v %)), x_2x_3, x_3x_4, x_3^2, and x_4^2 are significant variables ($p < 0.05$). The x_1, (ALG quantity) and x_4 (GAL-β-CD quantity) are the most significant variables affecting the GAL release concentration ($p < 0.0001$). Figure 1a and b show the normal plot and pareto chart showing the standardized effects of the factors on the response. According to the pareto chart, x_1 and x_4 above the reference line are the most important variables at a 95% confidence level. The results obtained from the pareto chart and normal plot are compatible with the results of the ANOVA analysis given in Table 4. ALG and GAL-β-CD are the most significant factors as they are the basic materials forming the hydrogel microparticle structure. However, x_1x_2, x_1x_3, x_1x_4, and x_2x_4 were found to be less effective variables ($p > 0.05$).

The surface analysis plots showing the effects and interaction of the significant factors (Time, $CaCl_2$ quantity, and

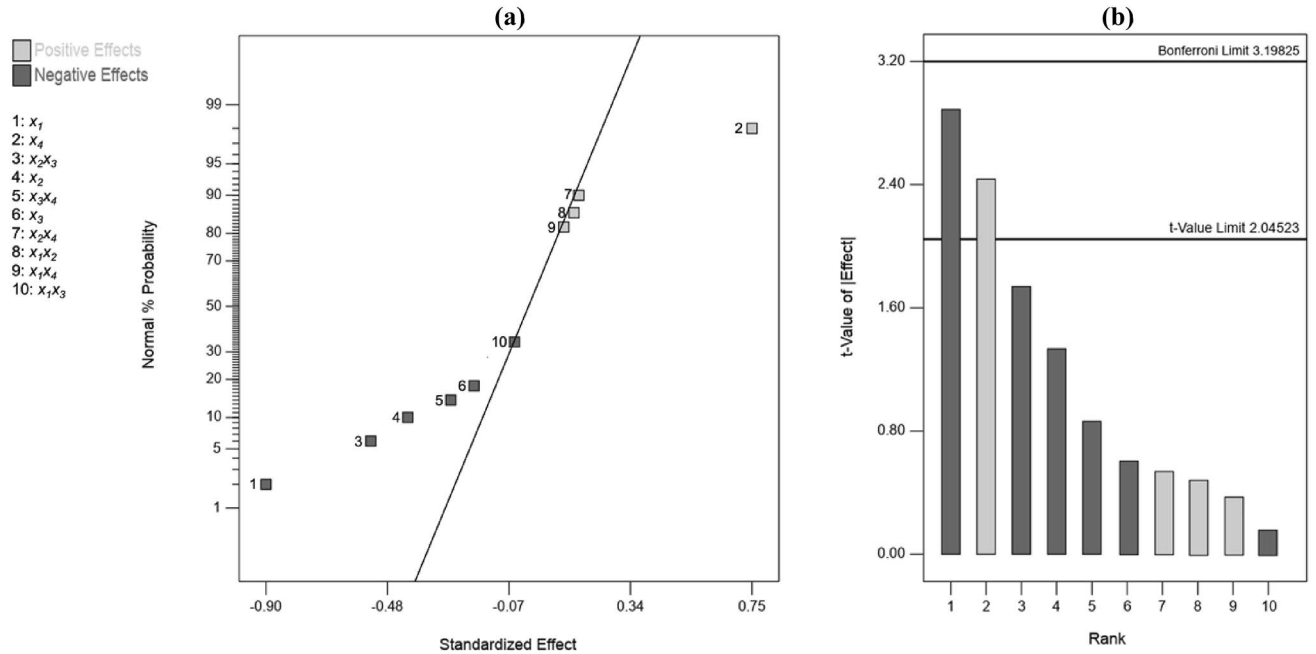


Fig. 1 **a** Normal plot of the standardized effects, **b** pareto plot of the standardized effects of a quadratic model

Table 5 Second order polynomial equations and regression coefficients of the response variables (ALG quantity x_1, $CaCl_2$ quantity x_2, the time x_3, the GAL-β-CD quantity x_4)

Responses	Second order polynomial equations
Concentration of released GAL (mg/L)	$y = 2.76 - 0.45x_1 - 0.21x_2 - 0.094x_3 + 0.38x_4 - 0.33x_2x_3 - 0.16x_3x_4 - 0.19x_3^2 - 0.29x_4^2$

GAL-β-CD quantity) on the GAL release concentration according to ANOVA analysis are given in Fig. 2a and b.

Figure 2a shows the effect of time and $CaCl_2$ quantity on the concentration of GAL released. The concentration of GAL released decreased with increasing time and the $CaCl_2$ quantity. On the contrary, the concentration of GAL released increases with decreasing time and the $CaCl_2$ quantity. As the cross-linker concentration decreases, the time required to form the hydrogel network decreases linearly. The best result was obtained at 1% $CaCl_2$ concentration versus time. 1% is the lowest level in the specified range of cross-linking agents. The cross-linker quantity is one of the most critical factors for producing cross-linked hydrogels because it forms bonds between polymer chains to form the hydrogel network. It can affect the structure of a polymeric network, limiting the elasticity and softness of hydrogels. As the amount of cross-linker increases, the amount of cross-links formed increases, and the polymeric structure becomes stiff and even brittle, resulting in a loss of softness and elasticity [49, 50]. Gomez et al., investigated the gelling efficiency of their synthesized ALG-β-CD derivative in the presence of calcium ions and compared with ALG. They found that the gelation efficiency of the ALG-β-CD derivative was higher than ALG, and as a result, the ALG-β-CD derivative formed softer gels. They reported that the reason for this was the decrease in the number of bonds between the polymer chains due to the steric hindrance of the ALG-β-CD derivative [51]. Also, as the cross-linking quantity increases, the water absorption capacity of hydrogels decreases. Therefore, their surface area reduces, and contact surfaces become narrow. Kozlowska et al., reported that water absorption capacity decreased with increasing stiffness in carrageenan-based hydrogels [52]. Hydrogels' elasticity, softness, and high water absorption capacity are the main reasons for their prevalent use in cosmetics [53]. The elasticity and softness of the obtained hydrogels indicate that a structure suitable for cosmetic applications has been developed.

Figure 2b shows the effect of time and GAL-β-CD on the concentration of GAL released. As the time decreases, the released GAL concentration increases. Similarly, as the amount of GAL-β-CD increases, the released GAL concentration increases and then decreases parabolically. The best result was obtained at 0.5% GAL-β-CD concentration versus time. When the GAL-β-CD quantity reached 0.5%, the amount of GAL released from the hydrogels started to decrease. The reason for this is predicted to reach the maximum amount that can be entrapped in the hydrogel network. Also, in this case, the amount of GAL released will be maximum, i.e., it will reach maximum solubility. The most critical fact in increasing the solubility of GAL is its entrapment in the hydrogels by embedding it in the hydrophobic cavity of β-CD. Kanjickal et al., developed hydrogels for cyclosporine carriers by two different methods. As the first method, they synthesized cyclosporine-loaded cross-linked PEG hydrogels. As the second method, they synthesized cyclosporine (2-hydroxypropyl)-γ-cyclodextrin inclusion complexes loaded cross-linked PEG hydrogels. They reported that the release profile of the inclusion complex loaded hydrogels was much more favorable than the release profile of directly loaded hydrogels since the release profile of the inclusion complex loaded hydrogels was controlled and slow [54]. Similarly, Omtvedt et al., compared the methyl orange release of alginate hydrogel beads grafted with β-CD inclusion complex and directly loaded alginate beads. They reported that the methyl orange release of alginate hydrogel beads grafted with β-CD inclusion complex was higher in a longer time than the methyl orange release of directly loaded alginate beads. β-CD inclusion complex grafted alginate beads release more because they can retain more methyl orange in the hydrogel network. The low capacity of alginate to retain small molecules causes difficult retention and leakage of the drug in the hydrogel network when direct drug loading is performed [55]. Abbas et al., developed a β-CD inclusion complex to increase the solubility of galangin and compared the release profile of the developed inclusion complex with free galangin under simulated physiological conditions. They reported that the galangin release rate of free galangin was 9.25%, and the inclusion complex reached 59.32%. The cavity inside the β-CD is hydrophobic, galangin settles in this cavity of the β-CD, and β-CD increases the solubility of galangin due to its hydrophilic outer surface [26].

Optimization of Hydrogel Generation Parameter

The optimum conditions, predicted, and experimental responses for the production of GAL-β-CD-ALG HMPs with maximum GAL release are given in Table 6. According to the table, the optimum conditions for hydrogel production are an ALG quantity 0.69%, $CaCl_2$ quantity 1.00%, a time 43.55 min, and GAL-β-CD quantity 0.48%. The predicted response for GAL release of GAL-β-CD-ALG HMPs prepared under the given optimum conditions is 4.97 mg/L, and the experimental response obtained is 5.02 ± 0.10 mg/L. Although the experimental response is slightly larger than the predicted response, the two responses are consistent, indicating that the model is valid and within the 95% confidence level. The CCD model, designed to produce GAL-β-CD-ALG HMPs with maximum GAL release capability, is accurate and reliable in predicting maximum GAL release.

Characterisation of Hydrogel Microparticles

SEM Analysis

The SEM image of GAL-β-CD and GAL-β-CD-ALG HMPs is given in Fig. 3. SEM analysis was used to

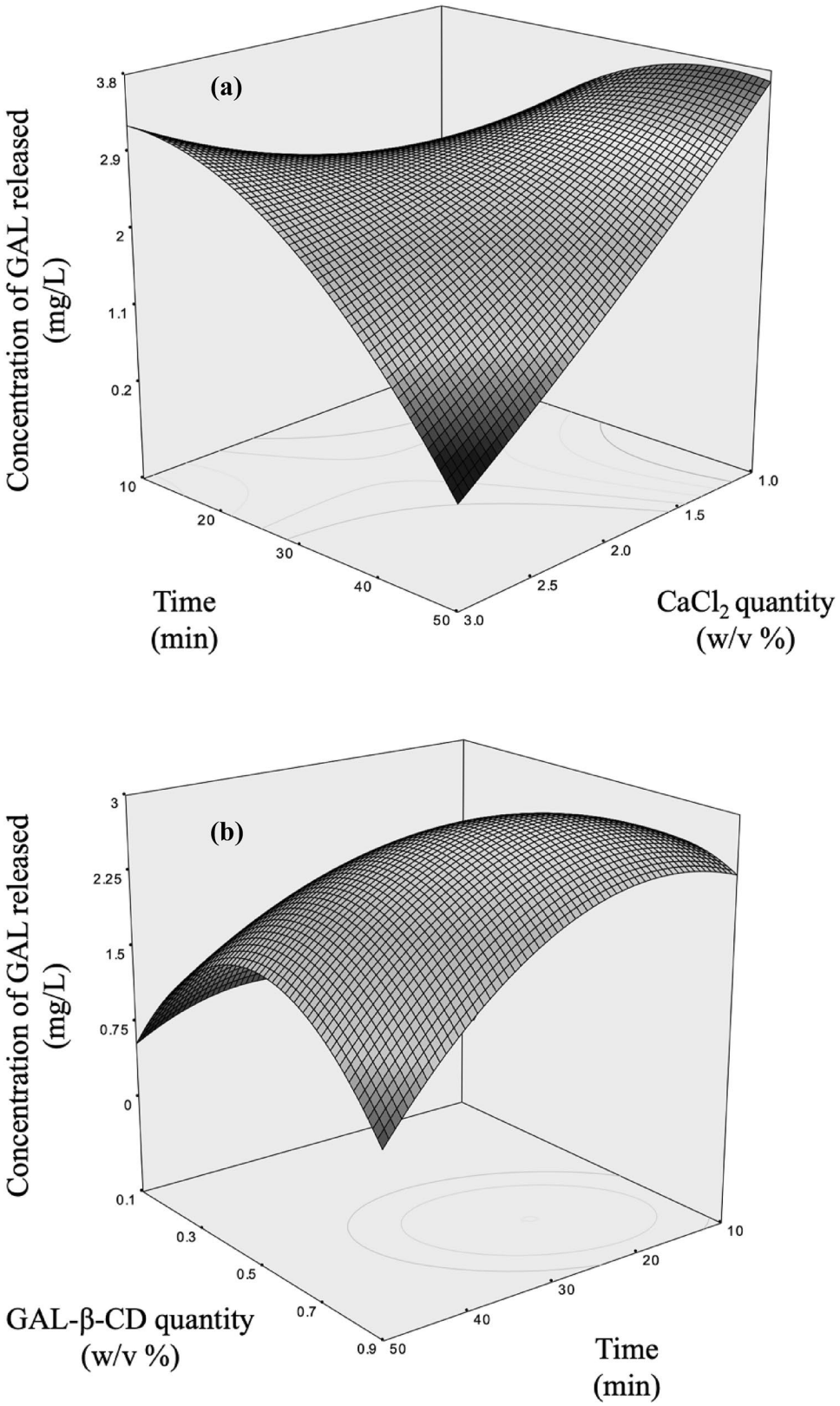


Fig. 2 Response surface plots of HMPs generation showing the effects of **a** Time (min) and $CaCl_2$ quantity (w/v %) and **b** GAL-β-CD quantity (w/v %) and Time (min) on the concentration of GAL release

Table 6 Optimum conditions predicted and experimental values of responses

Responses	Maximum values		Optimum encapsulation conditions			
	Predicted	Experimental	ALG quantity (w/v %)	$CaCl_2$ quantity (w/v %)	Time (min)	GAL-β-CD quantity (mg/L)
Concentration of released GAL (mg/L)	4.97	5.02 ± 0.10	0.69	1.00	43.55	0.48

determine the size of the GAL-β-CD-ALG HMPs and the average size of the GAL-β-CD-ALG HMPs was determined as 3.66 ± 0.59 µm. HMPs are in the range 1-1000 µm. The HMPs developed in this study are close to the lower limit of this range and agree with the literature. Mahmood et al., developed β-CD based hydrogel microparticles with sizes less than 1000 µm to increase the solubility of acyclovir. The developed HMPs increased the release of acyclovir due to the large surface area and wettability provided by its small size. Therefore, they reported that small particle size increases solubility [56]. The release of active substances from HMPs depends on particle size and shape [35]. Smaller particles are always preferred to improve and control the release of active substances due to their larger surface area [57]. Therefore, nano-sized hydrogel particles can be produced, but for cosmetic applications, mainly if the skin surface is targeted, micro-sized HMPs are advantageous [58]. For cosmetic purpose, Lin et al., developed 685.9-1044.4 µm alginate beads [59], Lebeer et al., developed 1500–2000 µm microcapsules [60], Shalaka et al., developed ~ 900 µm microspheres [61].

The morphological structure of GAL-β-CD appears clustered and branched. The main reason for the branched structure is based on the ability of β-CD to form complexes with aromatic structures of galangin. In GAL-β-CD-ALG HMPs, spherical and porous structures are observed. GAL-β-CD is localized in the polymer network of the inclusion complex and appears as spherical protrusions.

FTIR Analysis

The FTIR spectrum of GAL, β-CD, GAL-β-CD, ALG, and GAL-β-CD-ALG given in Fig. 4. In the FTIR spectrum of GAL, there are low intensity O–H stretching bands at 3503.81 and 3551.83 cm^{-1}, C=C stretching band at 3310.88 cm^{-1}, C=O stretching band at 1631.38 cm^{-1} and high intensity C–O stretching bands at 1160.81 cm^{-1}.

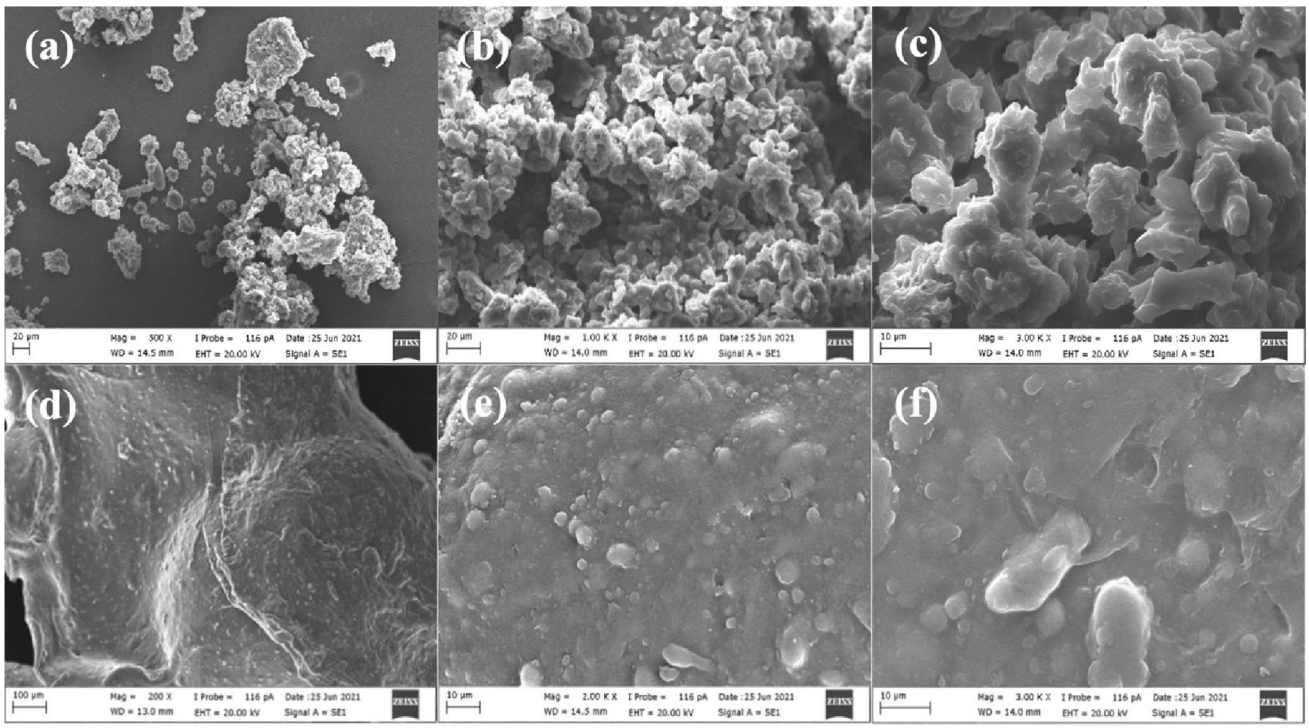


Fig. 3 The SEM image of **a** GAL-β-CD (500 X), **b** GAL-β-CD (1.00 KX), **c** GAL-β-CD (3.00 KX), **d** GAL-β-CD-ALG HMPs (200 X), **e** GAL-β-CD-ALG HMPs (2.00 KX), **f** GAL-β-CD-ALG HMPs (3.00 KX)

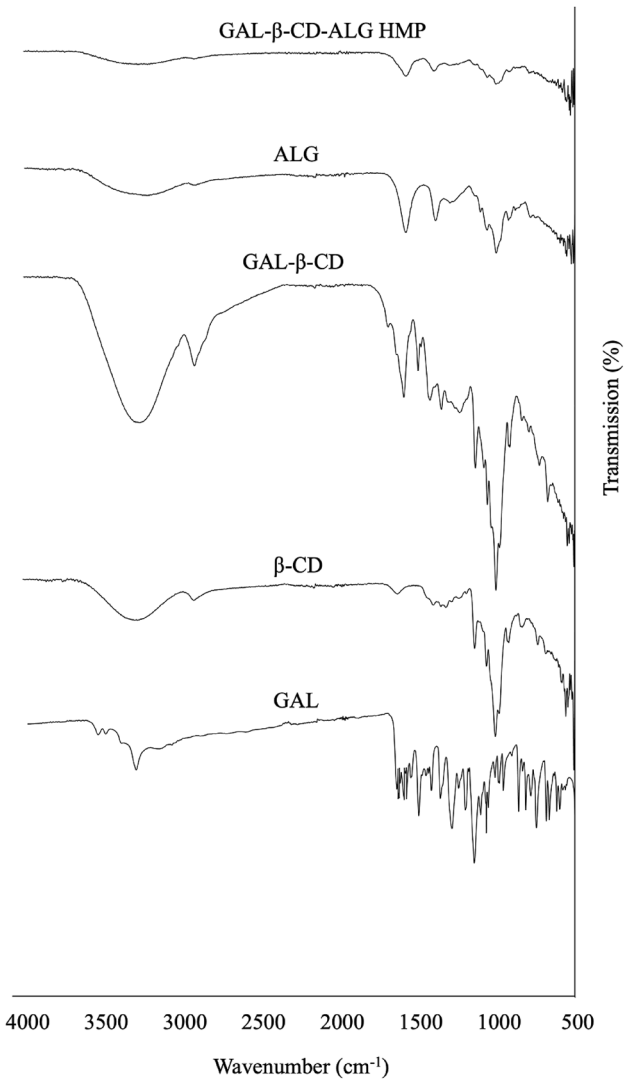


Fig. 4 FTIR spectra of GAL, β-CD, GAL-β-CD, ALG and GAL-β-CD-ALG HMPs

Looking at the FTIR spectrum of β-CD; the broadband frequency around 3000–3700 cm^{-1} indicates the presence of hydrogen bonding, i.e., OH group, the peak corresponding to the wave number 2900 cm^{-1} indicates sp^3 hybridization, and the fluctuation between 2000 and 2500 cm^{-1} indicates the presence of ring structure. The high intensity C=O streching band presence in 1022 and 1077 cm^{-1}. The spectrum of the GAL-β-CD mixture shows peaks at the same wave numbers as the others. This is because even if the molecular structures are not the same, they have similar structures and bonds. The most crucial point we should pay attention to is that the transmission ratios of the GAL-β-CD mixture seem lower than the others. The high intensity C=O stretching bands at 1025 and 1062 cm^{-1}, C–O stretching bands at 1606 cm^{-1} and the broad O–H stretching band at 3000–3700 cm^{-1} of GAL-β-CD are indicative of the inclusion complex between β-CD and GAL. Especially the broad O–H stretching band represents the presence of hydrogen bonds between the hydrophobic cavity of β-CD and GAL [26]. The FTIR spectrum of ALG; the band seen in the range of 3200–3300 cm^{-1} indicates the presence of an O–H bond, the peak at 2900 cm^{-1} indicates sp^3 hybridization, the fluctuation between 2000 and 2500 cm^{-1} indicates the presence of a ring structure, and the bands between 1600 and 1610 cm^{-1} are O–C–O carboxylate asymmetric stretching bands. In the FTIR spectrum of the GAL-β-CD-ALG structure, a broadband spectrum between 3000 and 3700 cm^{-1} is observed, i.e., the presence of a hydrogen-bonded (OH) group, the presence of sp^3 hybridization although 2900 cm^{-1} is a small peak, the vibrating peaks in the range of 2000–2500 cm^{-1} indicate the ring structure and the peak in the range of 1500–1700 cm^{-1} indicates the presence of aliphatic and aromatic double bonds.

Encapsulation Efficiency

Encapsulation efficiency is the primary indicator of the degree of success of the HMPs generation process. The encapsulation efficiency of the obtained GAL-β-CD loaded GAL-β-CD-ALG HMPs was determined as 91.5 ± 2.9%. The GAL-β-CD complex loaded into hydrogels contains 5.9781 mg GAL. The encapsulation efficiency of 91.5 ± 2.9% indicates that 5.47 mg of this GAL amount was loaded into the hydrogels. Galangin is a hydrophobic component, so its incorporation into polymeric networks of hydrophilic hydrogels is only possible using carrier systems. The loading of galangin with very high encapsulation efficiency into the polymeric network was achieved by embedding it in the hydrophobic cavity of the β-CD. Due to the high encapsulation efficiency, a higher amount of galangin will pass into a soluble form, and a higher amount of galangin will be released at the target site.

Conclusion

Galangin is a phenolic compound that can be widely used in cosmetic applications with its high antioxidant activity, anti-tyrosinase activity, anti-wrinkle effect, and anti-melanogenesis effect. However, due to its low solubility in water, oxidative instability, and low membrane permeability, its bioaccessibility and bioavailability are very poor, so its use in cosmetics is very limited. This study aimed to develop a novel and effective carrier system to increase the solubility and release of galangin. For this purpose, phenolic compounds were extracted from *Alpinia officinarum* Hance, from which a high proportion of galangin was purified and fractionated. In order to develop a hydrogel microparticle form of galangin that can be effectively used in cosmetic

formulations, hydrogel microparticle optimization was performed. In order to overcome the low solubility of galangin, a GAL-β-CD inclusion complex was formed and included in hydrogel microparticle formulations. The optimized hydrogel microparticles were produced with 91.5% encapsulation efficiency, 5.02 mg/L galangin release rate, 3.66 µm size, spherical shape, and soft texture suitable for cosmetic applications.

Author Contributions SŞ: Conceptualization; data curation; formal analysis; funding acquisition; investigation; methodology; resources; software; supervision; validation; visualization; writing—original draft; writing—review and editing.ÖA: Conceptualization; data curation; formal analysis; investigation; visualization; methodology. ED: Formal analysis; data curation; investigation; methodology. İP: Data curation; formal analysis; investigation; methodology; writing—review and editing.

Funding Open access funding provided by the Scientific and Technological Research Council of Türkiye (TÜBİTAK). The authors did not receive support from any organization for the submitted work.

Declarations

Conflict of interest The authors have no conflicts interests to declare that are relevant to the content of this article.

Open Access This article is licensed under a Creative Commons Attribution 4.0 International License, which permits use, sharing, adaptation, distribution and reproduction in any medium or format, as long as you give appropriate credit to the original author(s) and the source, provide a link to the Creative Commons licence, and indicate if changes were made. The images or other third party material in this article are included in the article's Creative Commons licence, unless indicated otherwise in a credit line to the material. If material is not included in the article's Creative Commons licence and your intended use is not permitted by statutory regulation or exceeds the permitted use, you will need to obtain permission directly from the copyright holder. To view a copy of this licence, visit http://creativecommons.org/licenses/by/4.0/.

References

1. Wang C, Chao I, Qin Y et al (2022) Comparison for quantification of eight components in *Alpinia officinarum* Hance by using high-performance liquid chromatography coupled with diode array detector and charged aerosol detector with individual and substitute reference compound. J Pharm Biomed Anal 210:114545. https://doi.org/10.1016/j.jpba.2021.114545
2. Nguyen TTA, Huynh DT, Rungraeng N (2019) Extraction and encapsulation of lesser galangal (Alpinia officinarum) essential oil using microwave pretreatment and spray drying. J Agric Environ Int Dev 18:57–63. https://doi.org/10.52997/jad.9.03.2019
3. Basri AM, Taha H, Ahmad N (2017) A review on the pharmacological activities and phytochemicals of *Alpinia officinarum* (Galangal) extracts derived from bioassay-guided fractionation and isolation. Pharmacogn Rev 11:43–56
4. Ye W, Sun W, Chen R et al (2019) Pharmacokinetics in rat plasma and tissue distribution in mice of galangin determined by UHPLC-MS/MS. Acta Chromatogr 31:120–125. https://doi.org/10.1556/1326.2017.00389
5. Sivakumar AS, Viswanathan P, Anuradha CV (2010) Dose-dependent effect of galangin on fructose-mediated insulin resistance and oxidative events in rat kidney. Redox Rep 15:224–232. https://doi.org/10.1179/135100010X12826446921545
6. Dixit A, Rohilla A, Dixit J, Singh V (2014) Qualitative analysis of various plant extracts of Alpinia officinarum. Int J Pharm Chem Biol Sci 4:505–508
7. Tao L, Wang ZT, Zhu EY et al (2006) HPLC analysis of bioactive flavonoids from the rhizome of Alpinia officinarum. S Afr J Bot 72:163–166. https://doi.org/10.1016/j.sajb.2005.06.007
8. Kale VM, Namdeo AG (2015) HPTLC densitometric evaluation by simultaneous estimation of galangin in Alpinia galanga and Alpinia officinarum. Der Pharm Lett 7:158–164
9. Choi JK, Kim SH (2014) Inhibitory effect of galangin on atopic dermatitis-like skin lesions. Food Chem Toxicol 68:135–141. https://doi.org/10.1016/j.fct.2014.03.021
10. Kim YJ, Lee EH, Cho EB et al (2019) Protective effects of galangin against UVB irradiation-induced photo-aging in CCD-986sk human skin fibroblasts. Appl Biol Chem 62:1–8. https://doi.org/10.1186/s13765-019-0443-3
11. Mak KK, Tan JJ, Marappan P et al (2018) Galangin's potential as a functional food ingredient. J Funct Foods 46:490–503. https://doi.org/10.1016/j.j.2018.04.054
12. Jailani F, Williamson G (2014) Effect of edible oils on quercetin, kaempferol and galangin transport and conjugation in the intestinal Caco-2/HT29-MTX co-culture model. Food Funct 5:653–662. https://doi.org/10.1039/c3fo60691k
13. Sabry S, El Hakim Ramadan A, Abd elghany M et al (2021) Formulation, characterization, and evaluation of the anti-tumor activity of nanosized galangin loaded niosomes on chemically induced hepatocellular carcinoma in rats. J Drug Deliv Sci Technol 61:102163. https://doi.org/10.1016/j.jddst.2020.102163
14. Karkar B, Patır İ, Şahin S (2023) Development of galangin-loaded nano-sized polyelectrolyte liposome: optimization and characterization. Polym Bull. https://doi.org/10.1007/s00289-023-04826-1
15. Landi-Librandi AP, Caleiro Seixas Azzolini AE, De Oliveira CA, Lucisano-Valim YM (2012) Inhibitory activity of liposomal flavonoids during oxidative metabolism of human neutrophils upon stimulation with immune complexes and phorbol ester. Drug Deliv 19:177–187. https://doi.org/10.3109/10717544.2012.679710
16. Landi-Librandi AP, De Oliveira CA, Caleiro Seixas Azzolini AE et al (2011) In vitro evaluation of the antioxidant activity of liposomal flavonols by the HRP-H2O2-luminol system. J Microencapsul 28:258–267. https://doi.org/10.3109/02652048.2011.559283
17. Zhu J, Wang Q, Li H et al (2018) Galangin-loaded, liver targeting liposomes: optimization and hepatoprotective efficacy. J Drug Deliv Sci Technol 46:339–347. https://doi.org/10.1016/j.jddst.2018.05.034
18. Yao H, Lu H, Zhang J et al (2019) Preparation of prolonged-circulating galangin-loaded liposomes and evaluation of antitumor efficacy in vitro and pharmacokinetics in vivo. J Nanomater. https://doi.org/10.1155/2019/7236895. 2019:2019
19. Patil S, Ujalambkar V, Rathore A et al (2019) Galangin loaded galactosylated pluronic F68 polymeric micelles for liver targeting. Biomed Pharmacother 112:108691. https://doi.org/10.1016/j.biopha.2019.108691
20. Zhu J, Wang Q, Zhu Y et al (2018) Enhanced oral bioavailability and in vivo hypouricemic activity of galangin via polymeric micelles. Lat Am J Pharm 37:1818–1827
21. Lu H, Chen X, Xu H (2021) Article Preparation of Galangin self-microemulsion drug delivery system and evaluation of its

pharmacokinetics in vivo and antioxidant activity in vitro. Pharmacogn Mag 18(80):1025–1034
22. Li Y, Guo M, Lin Z et al (2018) Multifunctional selenium nanoparticles with Galangin-induced HepG2 cell apoptosis through p38 and AKT signalling pathway. R Soc Open Sci 5:180509. https://doi.org/10.1098/rsos.180509
23. Mohammadi A, Kazemi S, Molayousefian I et al (2022) Galangin nanoparticles protect acetaminophen-induced liver injury: a biochemical and histopathological approach. J Evid Based Complementary Altern Med. https://doi.org/10.1155/2022/4619064. 2022:2022
24. Xiong Y, Wu B, Guo X et al (2023) Galangin delivered by retinoic acid-modified nanoparticles targeted hepatic stellate cells for the treatment of hepatic fibrosis. RSC Adv 13:10987–11001. https://doi.org/10.1039/d2ra07561j
25. Qaddoori MH, Al-Shmgani HS (2023) Galangin-Loaded gold nanoparticles: molecular mechanisms of antiangiogenesis properties in Breast cancer. Int J Breast Cancer. https://doi.org/10.1155/2023/3251211. 2023:2023
26. Abbas ZS, Sulaiman GM, Jabir MS et al (2022) Galangin/β-Cyclodextrin inclusion complex as a drug-delivery system for improved solubility and biocompatibility in Breast cancer treatment. Molecules 27:4521. https://doi.org/10.3390/molecules27144521
27. Jullian C (2009) Improvement of galangin solubility using native and derivative cyclodextrins: an UV-Vis and NMR study. J Chil Chem 54:201–203
28. Jeong D, Kim H, Jeong J et al (2016) Cyclosophoraose/cellulose hydrogels as an efficient delivery system for galangin, a hydrophobic antibacterial drug. Cellulose 23:2609–2625. https://doi.org/10.1007/s10570-016-0975-1
29. Zabot GL, Schaefer Rodrigues F, Polano Ody L et al (2022) Encapsulation of bioactive compounds for food and agricultural applications. Polymers 14:4194. https://doi.org/10.3390/polym14194194
30. Le Goff GC, Srinivas RL, Hill WA, Doyle PS (2015) Hydrogel microparticles for biosensing. Eur Polym J 72:386–412. https://doi.org/10.1016/j.eurpolymj.2015.02.022
31. Dcosta P, Shabaraya AR, Celvia Miranda F (2022) Hydrogel in novel drug delivery a review. Int J Pharm Res Appl 7:527. https://doi.org/10.35629/7781-0704527535
32. Cao H, Duan L, Zhang Y et al (2021) Current hydrogel advances in physicochemical and biological response-driven biomedical application diversity. Signal Transduct Target Ther 6:426. https://doi.org/10.1038/s41392-021-00830-x
33. Pirsa S, Khodaei SM, Karimi Sani I et al (2022) Hydrogels and biohydrogels: Investigation of origin of production, production methods, and application. Polym Bull 80:1–40. https://doi.org/10.1007/s00289-022-04580-w
34. Abasalizadeh F, Moghaddam SV, Alizadeh E et al (2020) Alginate-based hydrogels as drug delivery vehicles in cancer treatment and their applications in wound dressing and 3D bioprinting. J Biol Eng 14:1–22
35. Ahmad M, Rai SM, Mahmood A (2016) Hydrogel microparticles as an emerging tool in pharmaceutical field: a review. Adv Polym 35:121–128. https://doi.org/10.1002/adv.21535
36. Li J, Mooney DJ (2016) Designing hydrogels for controlled drug delivery. Nat Rev Mater 1:1–17. https://doi.org/10.1038/natrevmats.2016.71
37. Yang S, Wang F, Han H et al (2023) Fabricated technology of biomedical micro-nano hydrogel. Biomed Tech 2:31–48. https://doi.org/10.1016/j.bmt.2022.11.012
38. Ćorković I, Pichler A, Šimunović J, Kopjar M (2021) Hydrogels: characteristics and application as delivery systems of phenolic and aroma compounds. Foods 10:1252. https://doi.org/10.3390/foods10061252
39. Mitura S, Sionkowska A, Jaiswal A (2020) Biopolymers for hydrogels in cosmetics: review. J Mater Sci Mater Med 31:1–14. https://doi.org/10.1007/s10856-020-06390-w
40. Tu Y, Chen N, Li C et al (2019) Advances in injectable self-healing biomedical hydrogels. Acta Biomater 90:1–20. https://doi.org/10.1016/j.actbio.2019.03.057
41. Şahin S, Oran S, Şahintürk P et al (2015) Ramalina lichens and their major metabolites as possible natural antioxidant and antimicrobial agents. J Food Biochem 39:471–477. https://doi.org/10.1111/jfbc.12142
42. Karkar B, Şahin S (2022) Determination of phenolic compounds profiles and antioxidant properties of oleaster (Elaeagnus angustifolia L.) grown in Turkey. Eur Food Res Technol 248:219–241. https://doi.org/10.1007/s00217-021-03875-y
43. Şahin S, Ari F, Demir C, Ulukaya E (2014) Isolation of major phenolic compounds from the extracts of prunellal. Species grown in Turkey and their antioxidant and cytotoxic activities. J Food Biochem 38:248–257. https://doi.org/10.1111/jfbc.12043
44. Şahin S, Aybastier Ö, Işik E (2013) Optimisation of ultrasonic-assisted extraction of antioxidant compounds from Artemisia absinthium using response surface methodology. Food Chem 141:1361–1368. https://doi.org/10.1016/j.foodchem.2013.04.003
45. Aybastier Ö, Işik E, Şahin S, Demir C (2013) Optimization of ultrasonic-assisted extraction of antioxidant compounds from blackberry leaves using response surface methodology. Ind Crops Prod 44:558–565. https://doi.org/10.1016/j.indcrop.2012.09.022
46. Pirzadeh M, Barary M, Hosseini SM et al (2021) Ameliorative effect of Alpinia officinarum Hance extract on nonylphenol-induced reproductive toxicity in male rats. Andrologia 53:e14063. https://doi.org/10.1111/and.14063
47. Li CY, Cheng SE, Wang SH et al (2021) The anti-inflammatory effects of the bioactive compounds isolated from *Alpinia officinarum* Hance mediated by the suppression of NF-kappaB and MAPK signaling. Chin J Physiol 64:32–42. https://doi.org/10.4103/CJP.CJP_81_20
48. Fang L, Zhang H, Zhou J et al (2018) Rapid screening and preparative isolation of antioxidants from *Alpinia officinarum* Hance using HSCCC Coupled with DPPH-HPLC assay and evaluation of their antioxidant activities. J Anal Methods Chem. https://doi.org/10.1155/2018/3158293
49. Maitra J, Shukla VK, Kumar Shukla V (2014) Cross-linking in hydrogels-a review. Am J Polym Sci 2014:25–31. https://doi.org/10.5923/j.ajps.20140402.01
50. Al-Sibani M, Al-Harrasi A, Neubert RHH (2017) Effect of hyaluronic acid initial concentration on cross-linking efficiency of hyaluronic acid - based hydrogels used in biomedical and cosmetic applications. Pharmazie 72:81–86. https://doi.org/10.1691/ph.2017.6133
51. Gomez CG, Chambat G, Heyraud A et al (2006) Synthesis and characterization of a β-CD-alginate conjugate. Polymer 47:8509–8516. https://doi.org/10.1016/j.polymer.2006.10.011
52. Kozlowska J, Pauter K, Sionkowska A (2018) Carrageenan-based hydrogels: Effect of sorbitol and glycerin on the stability, swelling and mechanical properties. Polym Test 67:7–11. https://doi.org/10.1016/j.polymertesting.2018.02.016
53. Aswathy SH, Narendrakumar U, Manjubala I (2020) Commercial hydrogels for biomedical applications. Heliyon 6:e03719. https://doi.org/10.1016/j.heliyon.2020.e03719
54. Kanjickal D, Lopina S, Evancho-Chapman MM et al (2005) Improving delivery of hydrophobic Drugs from hydrogels through cyclodextrins. J Biomed Mater Res A 74:454–460. https://doi.org/10.1002/jbm.a.30374
55. Omtvedt LA, Dalheim M, Nielsen TT et al (2019) Efficient grafting of cyclodextrin to alginate and performance of the hydrogel

for release of model drug. Sci Rep 9:1–11. https://doi.org/10.1038/s41598-019-45761-4
56. Mahmood A, Ahmad M, Sarfraz RM, Minhas MU (2016) β-CD based hydrogel microparticulate system to improve the solubility of acyclovir: optimization through in-vitro, in-vivo and toxicological evaluation. J Drug Deliv Sci Technol 36:75–88. https://doi.org/10.1016/j.jddst.2016.09.005
57. Daly AC, Riley L, Segura T, Burdick JA (2020) Hydrogel microparticles for biomedical applications. Nat Rev Mater 5:20–43. https://doi.org/10.1038/s41578-019-0148-6
58. Łętocha A, Miastkowska M, Sikora E (2022) Preparation and characteristics of alginate microparticles for food, pharmaceutical and cosmetic applications. Polymers 14:3834. https://doi.org/10.3390/polym14183834
59. Lin SF, Chen YC, Chen RN et al (2016) Improving the stability of astaxanthin by microencapsulation in calcium alginate beads. PLOS ONE 11:e0153685. https://doi.org/10.1371/journal.pone.0153685
60. Lebeer S, Oerlemans E, Claes I (2018) Topical cream with live lactobacilli modulates the skin microbiome and reduce acne symptoms. BioRxiv. https://doi.org/10.1101/463307
61. Shalaka D, Amruta A, Parimal K (2009) Vitamin E loaded pectin alginate microspheres for cosmetic application. J Pharm Res 2:1098–1102

Publisher's Note Springer Nature remains neutral with regard to jurisdictional claims in published maps and institutional affiliations.